Effects of inelasticity on the apparent depth and detectability of seismic discontinuities in the mantle

Kelly H. Liu

Department of Geology, Kansas State University, Manhattan, Kansas, USA

Received 4 April 2002; revised 2 January 2003; accepted 29 January 2003; published 2 May 2003.

[1] Accurate determination of parameters about seismic discontinuities in the earth, such as their depth, existence, and strength, provides critical information about the physical and chemical states and dynamics of the earth's interior. Unfortunately, those parameters can be strongly affected by factors that are not related to the discontinuities. We use synthetic seismograms to estimate the influence of one of those factors, inelasticity, on the apparent depth and detectability of the 410- and 660- kilometer discontinuities obtained from stacking *P*-to-*S* converted phases (P_dS). Our results show that when P_dS travels through a zone with lower-than-normal Q values, the observed depth of discontinuities could be tens of kilometers deeper than the real value, and the stacking amplitudes and consequently the detectability and apparent strength are greatly reduced. This study demonstrates the importance of taking Q structure into account when seismologically detected discontinuity parameters are interpreted. *INDEX TERMS:* 7218 Seismology: Lithosphere and upper mantle; 7260 Seismology: Theory and modeling; 8120 Tectonophysics: Dynamics of lithosphere and mantle—general; 8124 Tectonophysics: Earth's interior—composition and state (1212). **Citation:** Liu, K. H., Effects of inelasticity on the apparent depth and detectability of seismic discontinuities in the mantle, *Geophys. Res. Lett.*, *30*(9), 1455, doi:10.1029/2002GL015264, 2003.

1. Introduction

[2] Seismic velocity discontinuities reflect rapid structural or mineralogical transitions in the earth. The two ubiquitous discontinuities that mark the top and bottom of the mantle transition zone are found at about 410 km and 660 km depth, respectively (hereafter referred to as *d*410 and *d*660). It is commonly believed that *d*410 is mostly caused by the phase transition from $(Mg, Fe)_2SiO_4$ (olivine) to its high-pressure polymorph β-spinel (wadsleyite), and *d*660 is mainly due to the phase transition of γ-spinel (ringwoodite) to $MgSiO_3$ (perovskite) and (Mg, Fe)O (magnesiowustite) [e.g., *Ringwood*, 1975; *Liu*, 1976, 1979; *Jackson*, 1983; *Ito et al.*, 1990; *Chudinovskikh and Boehler*, 2001]. The phase boundaries thought to produce *d*410 and *d*660 have positive and negative Clapeyron slopes, respectively. Therefore the amplitude of the uplift or depression of the discontinuities is an *in situ* measure of the temperature in the vicinity of the discontinuities.

[3] Over the past 40 years various seismological techniques have been developed to study seismic discontinuities in the mantle (for reviews, see *Bina* [1991] and *Helffrich* [2000]). Most of those techniques use body waves reflected, refracted, or converted from the discontinuities beneath the receiver, near the source, or at the mid-point between the receiver and the source. One of the most effective ways to image mantle discontinuities is to use teleseismic *P*-to-*S* converted phases (P_dS) from those discontinuities beneath a seismic station [*Dueker and Sheehan*, 1998; *Bostock*, 1998; *Chevrot et al.*, 1999; *Gao et al.*, 2002; *Kind et al.*, 2002; *Li et al.*, 2002]. Unfortunately, the apparent depth of *d*410 and *d*660, and consequently the transition zone thickness observed using such a technique (and most other techniques) can be significantly biased by the existence of velocity heterogeneities, seismic anisotropy, and anomalous Q along the ray-paths of the converted, reflected, or refracted waves. Those factors can also affect the detectability of a discontinuity by reducing or increasing the amplitude of the signal. Effects of velocity heterogeneities can be effectively corrected by using a local velocity model found by seismic tomography [*Dueker and Sheehan*, 1998], and those related to seismic anisotropy can be recognized by strong arrivals on the transverse component [*Bostock*, 1998]. Relative to velocity heterogeneities and anisotropy, the recognization and correction of the effects of Q on the observed depths and amplitudes of the discontinuities are less trivial.

[4] Q is a measure of the inelasticity of earth's material, and is commonly defined as the total energy over loss of energy per cycle [*Knopoff*, 1964], i.e., $Q = -2\pi E/\Delta E$. For a monochromatic plane wave with frequency f, the amplitude as a function of traveling distance is $A(x) = A_0 \exp[-\pi fx/(VQ)]$, where A_0 is the amplitude at distance $x = 0$, and V is the propagating velocity. Thus a wave with a higher frequency attenuates more rapidly than one with a lower frequency. A higher frequency wave also has a higher traveling velocity, which is given as $V(f)/V_0 = 1 + 1/(\pi Q)\ln(f/f_0)$ where f_0 is a reference frequency with velocity V_0 [*Aki and Richards*, 2002]. Therefore, seismic waves traveling through an inelastic medium suffer a phase delay due to frequency dispersion. The main frequencies of body waves on broadband seismograms (and the synthetic seismograms used in this study) range from 0.02 to 1.0 Hz, a band in which it is commonly believed that the Q values for most of the earth's materials are frequency-independent [*Knopoff*, 1964; *Lay and Wallace*, 1995].

[5] In the upper mantle and mantle transition zone, Q for *P*-waves, Q_p, is about twice as large as that for *S*-waves, i.e., $Q_p = 1.9Q_s$ [*Kanamori*, 1967], resulting in a stronger attenuation for *S*-waves than that for *P*-waves. In the 1-second PREM earth model [*Dziewonski and Anderson*, 1981], Q_p (Q_s) ranges from about 1350 (600) in the crust to about 200 (80) in the upper-most mantle from 35 to 210 km depth, and to about 360 (140) in the rest of the mantle above *d*660. It is

0094-8276/03/2002GL015264$05.00

generally believed that low-temperature structures such as subducted slabs correspond to high Q and high velocities [*Meyers et al.*, 1998], and structures with high temperature and especially partial melt such as mantle plumes and upwelling asthenosphere beneath active rifts [*Davis*, 1991] correspond to low Q and low velocities. While most tomographic results show that lateral velocity heterogeneity in the mantle is usually only a few percent, lateral variations of Q of more than 1000% in the mantle have been observed in various parts of the earth [*Lay and Wallace*, 1995].

[6] The apparent depths of discontinuities observed using P_dS are directly related to the arrival-time difference between the direct P-wave and the converted S-wave. Because of the differences in Q, velocities, and frequencies between P and S waves, the phase delay caused by inelasticity is expected to be different for P and P_dS. The difference in phase delay may result in an artificial bias of the observed depth of the discontinuities. In addition, the amplitude of P_dS and consequently the detectability and the apparent strength of a given discontinuity are also functions of the Q structure of the overlain layers. In this study we use synthetic seismograms to quantify the influence of Q anomalies on the observed depth of $d410$ and $d660$, as well as the stacking amplitudes of P_dS which are directly related to the detectability of the discontinuities.

2. Synthetic Seismograms

[7] We use CORE (Complete Ordered Ray Expansion) [*Clarke and Silver*, 1991] for the generation of synthetic seismograms. CORE is based on a ray-generation algorithm that involves the symbolic manipulation of complete body-wave wavefield expressions from reflectivity theory. Numerous tests show that the resulting broadband seismograms are in excellent agreement with full reflectivity synthetics and observed data [*Clarke and Silver*, 1991].

[8] We generate synthetic seismograms by using a set of models that are variants of the IASP91 earth model [*Kennett and Engdahl*, 1991], complemented with the Q values from PREM. The models are created by multiplying $Q_p(z)$ and $Q_s(z)$ in the PREM model by a set of constants, $R = Q(z)/Q(z)_{PREM}$, which range from 0.2 to 1.9. The large range of R is intended to be inclusive for extreme cases such as in the vicinity of subduction zones [e.g., *Meyers et al.*, 1998], and may not be representative for most part of the earth. Although in reality an anomaly in Q is usually accompanied by an anomaly in velocities, in this study we only vary $Q(z)$ in order to isolate the effects of inelasticity.

[9] We use three Q models to simulate different situations in the real earth. In the first model, $Q(z)$ values above $d660$ are modified; in the second model those between $d410$ and $d660$ are modified; and in the third model those above $d410$ are modified. To reduce computing time, four of the seven discontinuities in IASP91 at 35, 410, 660, and 2889 km depths are kept. In order to minimize the influence of source-side $Q(z)$ variation on the waveform, in this study we put an 'earthquake' at an unrealistic depth of 800 km. Synthetic seismograms are generated at 66 'stations', which are distributed in the epicentral distance range from 30° to 95° with a spacing of 1°. The source and the receivers are located along the same great circle arc.

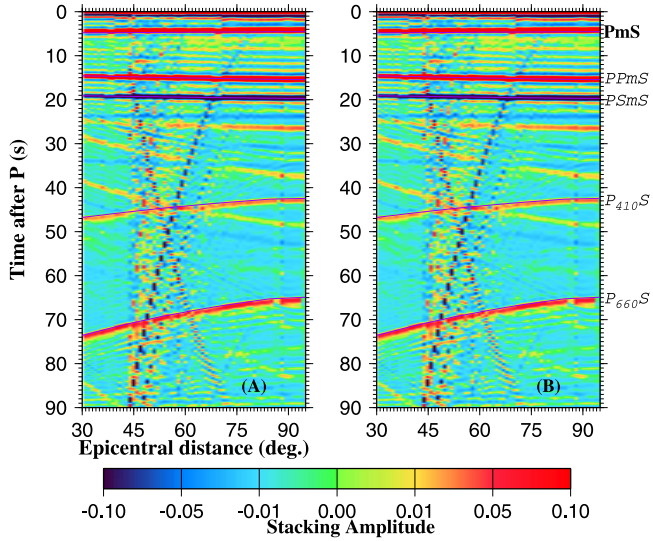

Figure 1. Radial receiver functions computed using synthetic seismograms for the second Q model for (A) R = 0.2 and (B) R = 1.9. The purple lines are theoretical arrivals calculated based on the IASP91 earth model.

3. Results

[10] To resemble the common practice in dealing with real data in discontinuity studies using P_dS, we deconvolve the radial components by the corresponding vertical components using the procedure of *Ammon et al.* [1990] to obtain receiver functions. Figure 1 shows receiver functions for two sets of synthetics when R = 0.2 and 1.9, respectively, for the second model, in which $Q(z)$ are modified in the depth range $410 \leq z \leq 660$ km. Because $Q(z)$ is not changed for $z \leq 410$ km, the phase delay of $P_{410}S$ is minimal, and the waveform is approximately the same for R = 0.2 and 1.9. On the other hand, the amplitude of $P_{660}S$ suffers a reduction in amplitude, and a clear phase delay is observed for R = 0.2 because $P_{660}S$ traveled through the mantle transition zone which has reduced $Q(z)$.

[11] We next stack the receiver functions by using the commom conversion point stacking procedure [*Dueker and Sheehan*, 1998].

[12] The procedure assumes a candidate discontinuity at a sequence of depths, and at each depth d, the travel time difference between the direct P-wave and the converted P_dS phase is calculated using [*Sheriff and Geldart*, 1982; *Gurrola et al.*, 1994]

$$T_{P_dS} = \int_{-d}^{0} \left[\sqrt{V_s(z)^{-2} - p^2} - \sqrt{V_p(z)^{-2} - p^2} \right] dz \qquad (1)$$

where p is the ray parameter for the P-wave, d is the depth of the candidate discontinuity, and $V_p(z)$ and $V_s(z)$ are the P- and S-wave velocities, as a function of depth, z. The receiver functions are then stacked using

$$A(d) = \frac{1}{N} \sum_{i=1}^{N} A_i\left(T_{P_dS}^{(i)}\right) \qquad (2)$$

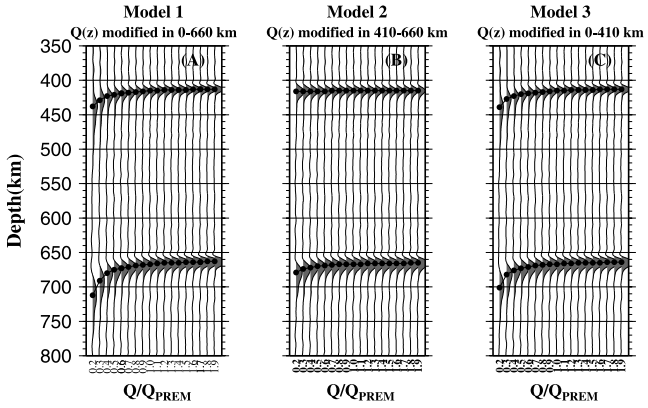

Figure 2. Results of phasing depth stacking of 66 radial receiver functions for a sequence of $Q(z)/Q(z)_{PREM}$ for the three Q models.

where $A(d)$ is the stacking amplitude for a candidate discontinuity at depth d, N is the number of stackings (i.e., the number of qualified receiver functions participated in the stacking), $T^{(i)}_{P_dS}$ is the P_dS moveout time of the ith receiver function for a discontinuity at depth d computed using equation (1), and $A_i(T^{(i)}_{P_dS})$ is the amplitude of the ith receiver function at time $T^{(i)}_{P_dS}$. Clearly, a real discontinuity corresponds to a large stacking amplitude. In this study the interval between the candidate discontinuities is taken as 1 km.

[13] The resulting phase depth images for the three Q models for a range of R are shown in Figure 2, and the corresponding transition zone thicknesses and the fitted results using a decaying exponential function are shown in Figure 3. For the first Q model, when $R < 1.0$, both $d410$ and $d660$ are significantly deeper than their true depths, due to the fact that both $P_{410}S$ and $P_{660}S$ are affected by the low Q. The apparent depths of $d410$ ($d660$) range from about 440 (710) km at $R = 0.2$ to its real depth of 410 (660) km for $R \geq 1.0$ (Figure 2A), and the transition zone thickness ranges from 274 km to its true value of 250 km (Figure 3A). For the second Q model, in which anomalous Q exists only

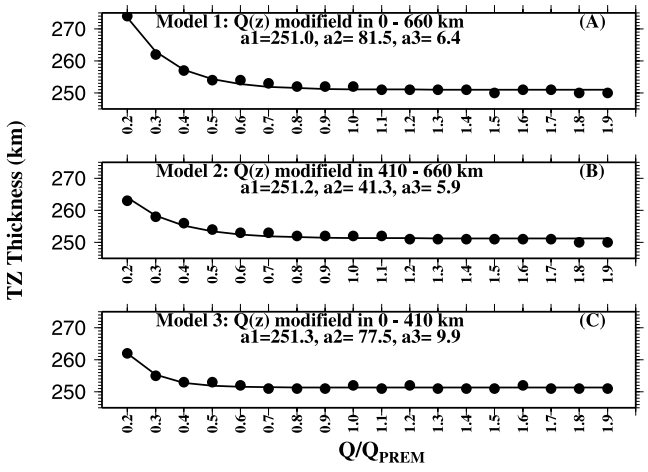

Figure 3. Transition zone thicknesses (dots) obtained from results shown in Figure 2 for the three Q models. The resolution of the observations is 1 km. The solid lines are fitted thicknesses using $a_1 + a_2 * \exp(-a_3 * R)$.

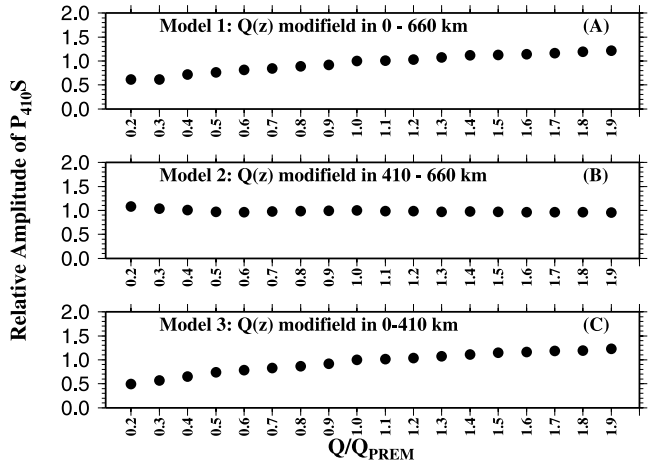

Figure 4. Amplitudes of $P_{410}S$ obtained from results shown in Figure 2. The values shown are stacking amplitudes relative to those of $R = 1.0$.

in the transition zone, the depth of $d410$ is not affected by R, and that of $d660$ ranges from 680 km when $R = 0.2$ to 660 km when $R \geq 1.0$ (Figure 2B). The thickness ranges from 263 km to 250 km (Figure 3B). Because anomalous Q exists only in the upper mantle in Model 3, for small R the apparent depth of both $d410$ and $d660$ are 20–40 km deeper than the true depths, and the transition zone thickness is about 10 km thicker than the true value (Figure 3C). The variation in apparent transition zone thickness for Model 3 is due to the fact that $P_{660}S$ travels a longer distance than $P_{410}S$ in the zone with anomalous Q (i.e., the upper mantle).

[14] Figure 4 shows the stacking amplitudes (normalized by those obtained for $R = 1.0$) of $P_{410}S$ as a function of R for the three Q models. For the first Q model, the amplitude increases from 0.6 for $R = 0.2$ to about 1.2 for $R = 1.9$; for the second Q model, it is approximately independent of R; and for the third Q model, it varies from about 0.5 to 1.2. The amplitudes for $P_{660}S$ increase with R for all the three Q models (Figure 5), from about 0.35 (0.6 and 0.4) at $R = 0.2$ to about 1.4 (1.1 and 1.2) at $R = 1.9$ for the first (second and third) Q model.

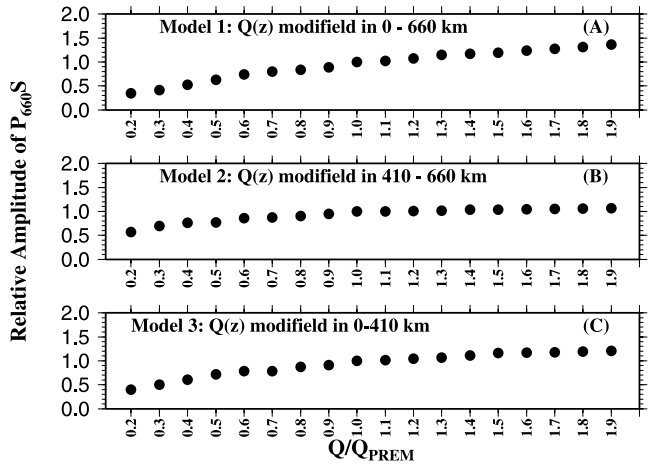

Figure 5. Same as Figure 4 but for $P_{660}S$.

4. Discussion and Conclusions

[15] Results presented above demonstrate the significant influence of low-Q zones in the upper mantle and mantle transition zone on the observed time delay and amplitude of P-to-S converted phases. In order to make sensible interpretations of results obtained by stacking P-to-S converted phases, the effect of low-Q zones must be identified and, more ideally, corrected.

[16] The most efficient way to estimate the influence of low-Q zones on the apparent depths and detectability of discontinuities is to perform an independent measurement of the Q structure. Beneath dense seismic arrays, relative attenuation can be measured using the spectral ratio [*Teng*, 1968] or other [e.g., *Gao*, 1997] methods, and Q anomalies beneath an isolated station can be obtained by computing spectral ratios between observed and synthetic seismograms using events with various azimuths and distances, or by using phases with different ray-paths [*Reid et al.*, 2001]. Once the Q structure is determined, the influence of Q can be corrected by minimizing the Q effects on the seismograms [*Tanaka and Hamaguchi*, 1992] prior to the computation of receiver functions. Such a correction must be applied carefully when the effects of velocity variation on discontinuity depth are also corrected. It is well-known that a low velocity layer leads to a delay in the arrival time of the entire wave train, while a low Q layer results in a broadening of the pulses accompanied by a shift and reduction of the peak amplitude. In principle, for a pair of near-by stations, the relative travel time (δt) and relative t^* (i.e., travel time over Q) can be obtained by simultaneously correcting for the attenuation effects and shifting the seismograms [*Stark and Forsyth*, 1983; *Tanaka and Hamaguchi*, 1992]. In practice, however, some seismic tomography studies assume a laterally homogeneous $Q(z)$ beneath a regional seismic network, and the phase delay resulting from low Q is interpreted as the consequence of an apparent low velocity zone. Thus, when the depth of the seismic discontinuities is corrected using a local velocity model obtained under the homogeneous Q assumption, the phase delay resulting from low Q will be partially accounted for. An additional correction for Q structure will lead to over-correction of the depth of the discontinuities.

[17] Because of the strong reduction of stacking amplitude when R is small (Figures 4 and 5), the detectability of the discontinuities can be significantly affected by the Q structure of the earth above the discontinuities. Therefore, a distinction must be made between the non-existence of a particular discontinuity and the consequence of a reduced detectability due to low Q. In addition, because of the strong influence of low Q on the apparent amplitudes of the discontinuities, the velocity contrasts obtained from the stacking amplitudes can also be affected, resulting in under-estimated values.

[18] **Acknowledgments.** The author thanks Tim Clarke and Paul Silver for providing the CORE suite of programs, and Steve Gao for discussion. This research was supported by National Science Foundation grants EAR-0001000 and EAR-0107055.

References

Aki, K., and P. G. Richards, *Quantitative Seismology*, 2nd ed., Univ. Sci., Sansalito, Calif., 2002.

Ammon, C. J., G. E. Randall, and G. Zandt, On the nonuniqueness of receiver function inversions, *J. Geophys. Res.*, *95*, 15,303–15,318, 1990.

Bina, C. R., Mantle discontinuities, *Rev. Geophys.*, *29*, 783–793, 1991.

Bostock, M. G., Mantle stratigraphy and evolution of the Slave province, *J. Geophys. Res.*, *103*, 21,183–21,200, 1998.

Chevrot, S., L. Vinnik, and J. P. Montagner, Global-scale analysis of the mantle Pds phases, *J. Geophys. Res.*, *104*, 20,203–20,219, 1999.

Chudinovskikh, L., and R. Boehler, High-pressure polymorphs of olivine and the 660-km seismic discontinuity, *Nature*, *411*, 574–577, 2001.

Clarke, T. J., and P. G. Silver, A procedure for the systematic interpretation of body wave seismograms I. Application to Moho depth and crustal properties, *Geophys. J. Int.*, *104*, 41–72, 1991.

Davis, P. M., Continental rift structures and dynamics with reference to teleseismic studies of the Rio Grande and East African rifts, *Tectonophysics*, *197*, 309–325, 1991.

Dueker, K. G., and A. F. Sheehan, Mantle discontinuity structure beneath the Colorado Rocky Mountains and High Plains, *J. Geophys. Res.*, *103*, 7153–7169, 1998.

Dziewonski, A. M., and D. L. Anderson, Preliminary reference earth model, *Phys. Earth Planet. Inter.*, *25*, 297–365, 1981.

Gao, S. S., A Bayesian approach for the calculation of seismic body-wave attenuation factors, *Bull. Seismol. Soc. Am.*, *87*, 961–970, 1997.

Gao, S. S., P. G. Silver, K. H. Liu, and the Kaapvaal Seismic Group, Mantle discontinuities beneath southern Africa, *Geophys. Res. Lett.*, *29*(10), 1491, doi:10.1029/2001GL013834, 2002.

Gurrola, H., J. B. Minster, and T. Owens, The use of velocity spectrum for stacking receiver functions and imaging upper mantle discontinuities, *Geophys. J. Int.*, *117*, 427–440, 1994.

Helffrich, G., Topography of the transition zone seismic discontinuities, *Rev. Geophys.*, *38*, 141–158, 2000.

Ito, E., M. Akaogi, L. Topor, and A. Navrotsky, Negative pressure-temperature slopes for reactions forming $MgSiO_3$ perovskite from calorimetry, *Science*, *249*, 1275–1278, 1990.

Jackson, I., Some geophysical constraints on the chemical composition of the Earth's lower mantle, *Earth Planet. Sci. Lett.*, *62*, 91–103, 1983.

Kanamori, H., Spectrum of P and PcP in relation to the mantle-core boundary and attenuation in the mantle, *J. Geophys. Res.*, *72*, 559–571, 1967.

Kennett, B. L. N., and E. R. Engdahl, Traveltimes for global earthquake location and phase identification, *Geophys. J. Int.*, *105*, 429–465, 1991.

Kind, R., X. Yuan, J. Saul, and D. Nelson, Seismic images of crust and upper mantle beneath Tibet: Evidence for Eurasian plate subduction, *Science*, *298*, 1219–1221, 2002.

Knopoff, L., *Q*, *Rev. Geophys.*, *2*, 625–660, 1964.

Lay, T., and T. C. Wallace, *Modern Global Seismology*, Academic, San Diego, Calif., 1995.

Li, A., K. M. Fischer, S. van der Lee, and M. E. Wysession, Crust and upper mantle discontinuity structure beneath eastern North America, *J. Geophys. Res.*, *107*(B5), 2100, doi:10.1029/2001JB000190, 2002.

Liu, L.-G., The post-spinel phase of forsterite, *Nature*, *262*, 770–772, 1976.

Liu, L.-G., Phase transformations and the constitution of the deep mantle, in *The Earth: Its Origin, Structure and Evolution*, edited by M. W. McElhinny, pp. 177–202, Academic, San Diego, Calif., 1979.

Meyers, S. C., S. Beck, G. Zandt, and T. Wallace, Lithospheric-scale structure across the Bolivian Andes from tomographic images of velocity and attenuation for P and S waves, *J. Geophys. Res.*, *103*, 21,233–21,252, 1998.

Reid, F. J. L., J. H. Woodhouse, and H. J. van Heijst, Upper mantle attenuation and velocity structure from measurements of differential S phases, *Geophys. J. Int.*, *145*, 615–630, 2001.

Ringwood, A. E., *Composition and Petrology of the Earth's Mantle*, 604 pp., McGraw-Hill, New York, 1975.

Sheriff, R. E., and L. P. Geldart, *Exploration Seismology*, Cambridge Univ. Press, New York, 1982.

Stark, M., and D. W. Forsyth, The geoid, small-scale convection, and differential travel time anomalies of shear waves in the central Indian Ocean, *J. Geophys. Res.*, *88*, 2273–2288, 1983.

Tanaka, S., and H. Hamaguchi, Heterogeneity in the lower mantle beneath Africa, as revealed from S and ScS phases, *Tectonophysics*, *209*, 213–222, 1992.

Teng, T. L., Attenuation of body waves and the Q structure of the mantle, *J. Geophys. Res.*, *73*, 2195–2208, 1968.

K. H. Liu, Department of Geology, Kansas State University, Manhattan, KS 66506, USA. (liu@ksu.edu)